Uncertainties in shoreline position analysis: the role of run-up and tide in a gentle slope beach

Giorgio Manno[1], Carlo Lo Re[1], and Giuseppe Ciraolo[1]

[1]Department of Civil, Environmental, Aerospace, Materials Engineering – University of Palermo, Viale delle Scienze, Ed. 8, 90128 Palermo (PA)

Correspondence to: Carlo Lo Re (carlo.lore@unipa.it)

Abstract. In the last decades in the Mediterranean sea, high anthropic pressure from increasing economic and touristic development has affected several coastal areas. Today the erosion phenomena threaten human activities and existing structures, and interdisciplinary studies are needed to better understand actual coastal dynamics. Beach evolution analysis can be conducted using GIS methodologies, such as the well-known Digital Shoreline Analysis System (DSAS), in which error assessment based on shoreline positioning plays a significant role. In this study, a new approach is proposed to estimate the positioning errors due to tide and wave run-up influence. To improve the assessment of the wave run-up uncertainty, a spectral numerical model was used to propagate waves from deep to intermediate water and a Boussinesq-type model for intermediate water up to the swash zone. Tide effects on the uncertainty of shoreline position were evaluated using data collected by a nearby tide gauge. The proposed methodology was applied to an unprotected, dissipative Sicilian beach far from harbours and subjected to intense human activities over the last 20 years. The results show wave run-up and tide errors ranging from 0.12 m to 4.5 m and from 1.20 m to 1.39 m, respectively.

1 Introduction

Mediterranean beaches are well known for their high environmental, economic and sociocultural value. In the last few decades, most of these beaches have been subjected to demographic growth from increasing tourism and commercial activities (Cooper et al., 2009). To support these activities, new defence structures have been built along some beaches, and although these structures have reduced local erosive effects, they have also increased erosion on neighbouring coasts (e.g., Griggs, 2005; Stancheva et al., 2011; Manno et al., 2016). Coastal erosion is a relevant problem that involves both socio economic resources and private properties, and its assessment has long been an issue of international interest involving political decision-makers and researchers (Douglas and Crowell, 2000; Phillips and Jones, 2006; Anfuso et al., 2011; Rangel Buitrago and Anfuso, 2015). Historical beach evolution, erosion, and the retreat/accretion of shoreline has been analysed using aerial and satellite images (e.g., Thieler et al., 2009; Fletcher et al., 2003; Genz et al., 2007; Anfuso et al., 2011; Dolan et al., 1980, 1991). Each remote image is often used to represent a year, and therefore the "shoreline" position identified and digitalized from each image, becomes representative of all shoreline positions in that specific year. The Coastal Engineering Manual (U.S. Army, 2008) defines "shoreline" as the intersection between land and water body, but to choose a suitable proxy that accounts

for the spatial and time variability (Bush et al., 1999), this boundary must be localized. Among different shoreline proxies (Boak and Turner, 2005), the wet/dry boundary is clearly identified in aerial images by the different colours of sand during the drying process. Because it is more sensitive to run-up fluctuations than astronomical tide variations (Dolan et al., 1980), the wet/dry boundary is a stable shoreline proxy that has been applied by several authors for various applications regarding

5   localization and analysis of shoreline (e.g. Pajak and Leatherman, 2002; Moore, 2000; Moore et al., 2006; Stockdon et al., 2002; Robertson et al., 2004). Thieler et al. (2009) developed a method to assess the beach evolution trend by means of aerial imageries, implemented in a software extension to ESRI ArcGIS© v.9+, the Digital Shoreline Analysis System (DSAS), that can calculate the shoreline rate-of-change statistics starting from multiple historical shoreline positions. This method has the advantage of considering uncertainties due to positioning and measurements errors (Fletcher et al., 2003). The positioning

10   errors are strictly connected to physical phenomena and can affect the analysis precision because the erroneous position of shoreline is assumed as "actual" for the considered year. Uncertainties from tides and wave storms (seasonal variability) are linked to the "exact position" of shoreline during the aerial shooting (Fletcher et al., 2003), whereas measurement uncertainties are linked to errors of image processing and digitizing conducted by technicians who identify and map the shoreline position for several observation years (Fletcher et al., 2003). Several authors (Genz et al., 2007; Rooney et al., 2003; Romine and Fletcher,

15   2012) used DSAS to evaluate both positioning errors and measurement errors, neglecting the error due to wave run-up and astronomic tide fluctuations. By contrast, other authors (e.g. Virdis et al., 2012; Manca et al., 2013) added to the positioning uncertainty the effects due to wave motion, calculating the run-up by means of the empirical formula of Hunt (1959). In this paper, an interdisciplinary method that more accurately assesses shoreline positioning error caused by wave run-up and tidal fluctuations in DSAS analysis is presented. Wave run-up was calculated using a numerical model cascade, which includes a

20   wave spectral model and a shallow water propagation model. Tide effects were evaluated using the daily variation of astronomic and meteorological tide. With this method, a dissipative sandy beach of the western coast of Sicily (Italy) was analysed, an interesting case study because, in the last decades, it has been heavily impacted by human activities. This beach represents a practical case in which accurate identification of the shoreline position with extreme fluctuations is fundamental to forecasting inundation areas or planning effective beach management practices.

2   Methodology

The methodological goal was to better evaluate positioning errors caused by wave run-up and tide for DSAS applications, an ArcGIS extension used to compute the shoreline rate-of-change (Thieler et al., 2009). The latter was evaluated by five different methods to compare the related results. The first method considered the end point rate (EPR), calculated by dividing the shoreline shift by the time elapsed between the oldest and the most recent shoreline position. The second method used the

30   linear regression rate (LRR) of change based on the determination of least-squares regression lines of all the shoreline points of

each transect. The third method used a weighted linear regression (WLR), in which the weight w is a function of the variance of the measurement uncertainty (Thieler et al., 2009): eq. (1):

$$w = 1/e^2 \tag{1}$$

where e is the shoreline uncertainty value. The fourth and fifth methods are based on the analysis of distances rather than rates. The fourth method considers the "net shoreline movement" (NSM), the distance between the oldest and youngest shoreline position for each transect, and the fifth considers the "shoreline change envelope" (SCE), the distance between the farthest and closest shorelines to the baseline at each transect. To assess the total uncertainty (σ_T) affecting each shoreline position, the following relationship was assumed (Virdis et al., 2012):

$$\sigma_T = \pm\sqrt{\sigma_d^2 + \sigma_p^2 + \sigma_r^2 + \sigma_{co}^2 + \sigma_{wr}^2 + \sigma_{td}^2} \tag{2}$$

where the uncertainty σ_i is the standard deviation of the i-type error; σ_d is the digitizing error determined by digitizing several times the same feature on the image; σ_r is the orthorectification error, considered as the root mean square error (RMSE) for photogrammetric blocks; σ_{co} is the image coregistration error arising from the RMSE of misalignment between single pixels from the set of images obtained by the rectification; σ_p is the pixel error assumed equal to the pixel size; and σ_{wr} and σ_{td} are, respectively, the wave run-up and the tide errors estimated in this study (discussed later). Note that the first four errors are related to intrinsic characteristics of the used images, how they were taken and how they were processed, whereas the last two are related to specific geomorphologic, mareographic, and wave characteristics of the beach examined. Variables σ_{td} and σ_{wr} represent position errors that may result in noticeably higher values than the others, therefore special care is required during their evaluation, which is the focus of this study.

To improve the evaluation of the wave run-up and tide uncertainty (σ_{wr}, σ_{td}) with respect to the use of empirical formulas found in the technical literature (e.g. Virdis et al., 2012; Manca et al., 2013), various mathematical models were applied. An hydraulic study, conducted on the basis of a geomorphologic study, determined the effects of wave motion and tide fluctuation on the shoreline position. To this aim, offshore wave parameters were used to simulate wave propagation from deep water to run-up on the beach, whereas a tide-gauge dataset was used for analysis of tide fluctuation. The whole mathematical process for the run-up calculation can be summarized by the following steps: a) select offshore buoy dataset collection; b) propagate waves from deep to intermediate water by means of a wave spectral model; c) generate random waves from a JONSWAP spectrum; d) propagate waves from intermediate water up to the swash zone with a Boussinesq-type model; and e) conduct run-up analysis. This mathematical process has been validated using in field measurements as described in the Section 4. The Boussinesq-type model considered in the present paper is able to propagate the waves from a relatively small water depth ($kh = 0.7$ where k is the wave number and h is the local water depth) up to the shoreline. Assuming a JONSWAP spectrum, the significant wave height and wave period were converted into the time series of an energetically equivalent irregular wave train, which was then propagated using the shoreline Lagrangian numerical model of Lo Re et al. (2012b). In the shoreline model, a Boussinesq

type model for breaking waves with the governing equations solved in the $\zeta - u$ form was implemented, where ζ is the free surface elevation and u is the depth-averaged horizontal velocity. The values of the variables ζ e u were calculated inside the wet domain, whereas the shoreline position (defined by means of its horizontal coordinate $\xi(t)$ perpendicular to the coast) and its velocity u_s were calculated by means of the Lagrangian shoreline equations. In the case of an orthogonal wave attack as the one considered here, the variable ξ is only function of time, i.e. $\xi = \xi(t)$ and the kinematic condition at the shoreline is the following:

$$\frac{d\xi}{dt} = u_s \tag{3}$$

Such a relation states that the fluid particles at the shoreline remain along the shoreline. Moreover the momentum equation at the shoreline that must be also be considered in order to close the problem in dimensional form reads:

$$\frac{du_s}{dt} = -g\frac{\partial \zeta}{\partial x}\Big|_s + F_{fric} \tag{4}$$

where $\partial \zeta / \partial x|_s$ is the derivative of the surface elevation evaluated at the shoreline and F_{fric} is the bottom friction force, evaluated as follows:

$$F_{fric} = \frac{f}{h+\zeta} \cdot u \cdot |u| \tag{5}$$

in which h is the local depth and f is the bottom friction coefficient. When the value of F_{fric} becomes too large, due to the small value of the total water depth, a threshold is used. In such a case, the dependency on the water depth is eliminated and the bottom friction is assumed to be only a quadratic function of the depth-averaged velocity:

$$F_{fric} = C_f \cdot u \cdot |u| \tag{6}$$

where C_f is a coefficient that was assumed equal to 5.0 m^{-1}.

The propagation of the offshore wave characteristics to shallow water was carried out by the well-known SWAN spectral propagation model (Booij et al., 1999; Holthuijsen et al., 1993; Ris et al., 1999).The SWAN results obtained for the 5 m bathymetric line were then used as input for the Boussinesq-type model by Lo Re et al. (2012b) which, coupled with a specific Lagrangian model for shoreline movement, allowed simulation of wave swash and run-up. The wave run-up error σ_{wr} was finally estimated by analysing the resulting shoreline movement over time. Note that the offshore wave parameters were the only source in the propagation model SWAN. Moreover because the SWAN simulation covers a small region in intermediate water, the wind input, the wave drop due to white-capping, and the wave drop due to bottom friction were not considered (Rusu, 2009). Indeed, in large deep water regions with very shallow water the wind and the bottom friction could play a significant role and cannot be neglected. For wave propagation by SWAN, a 2D unstructured grid following the Delaunay rule was implemented, constructed in accordance with Monteforte et al. (2015) using a density function in which the triangle sizes

depended on local water depth and wavelength. The node elevation was calculated by a linear interpolation of bathymetric data from nautical charts. The Lagrangian model used for shoreline movement discriminates between wet and dry regions to simulate run-up and run-down along surveyed sections. For the ith section the standard deviation of the horizontal shoreline movement over time was calculated by:

$$\sigma_{w,i} = \frac{S_{wr,i}}{\tan \alpha_i} \tag{7}$$

where $S_{wr,i}$ is the standard deviation of the vertical shoreline fluctuation computed by the model, and $\tan \alpha_i$ is the section slope. Finally, the wave run-up error for the whole beach σ_{wr} was estimated by:

$$\sigma_{wr} = \sqrt{\frac{\sigma_{wr,1}^2 + \sigma_{wr,2}^2 + ... + \sigma_{wr,n}^2}{(n-1)}} \tag{8}$$

The tide uncertainty σ_{td} was assessed by processing the tide measurements recorded by a mareographic station. For each year with measures, the standard deviation of the tide measurements, S_{td}, was first computed, and the standard deviations of the horizontal tidal fluctuations of the same sections used for run-up assess were then evaluated using an equation formally identical to Eq. (7). The tide uncertainty for the whole beach, σ_{td}, was finally assessed with the same equation used for the run-up error (Eq. (8)).

3   The case study: *Marsala* beach

The case study of the dissipative beach (Fig. 1), *Lido Signorino*, extends in a north–south direction for about 3.5 km between Cape Torre Tunna and Cape Torre Sibilliana. Its slope ranges between 1.5° and 10.8° and the direction of beach exposure (Fig. 1) is about 140°, between NW and S-SW. The *Egadi* Islands, in particular *Favignana* Island, shield the beach in the 320° N direction. The geographical fetch is limited from the west by the Spanish coast, from the south by the African coast and from the north-west by the Sardinian coast.

The buoy belongs to the Italian Wave Buoy Network (RON) and the rose, obtained by processing available data recorded from July 1989 to June 2012, shows that the most intense and most numerous waves come from around 270° N, 290° N and 292.5° N. The beach is made of fine carbonatic sand (Holocene) with sub-smoothed lithic and fossil shells grains Manno et al. (2011). The granulometric analysis indicates $D_{50} = 0.42$ mm, and a uniformity coefficient of 2.75 mm. The granulometric fractions are 0.4% silt, 0.6% clay, and 99% sand. The sediment has effective porosity of about 26% and high permeability ranging between 10^{-2} and $5 \cdot 10^{-3}$ cm s^{-1}.

The beach suffers from intense anthropogenic use, especially houses placed too close to the shoreline (Fig. 2), which has caused progressive destruction of dunes and their associated natural supply. In the first 50 years of the 20th century, the dunes were uniform from north to south and about 5 m high, whereas today they are discontinuous, about 2.5 m high and mainly located in the less developed southern area.
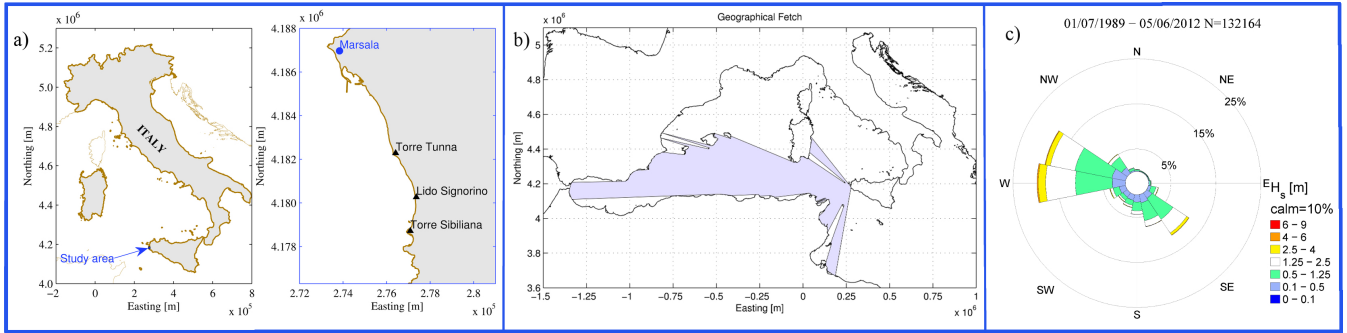
Figure 1. a) Map of Italy (left panel) and of the study area (right panel), showing the locations of Cape *Torre Tunna*, Cape *Torre Sibilliana*, *Lido Signorino* beach and *Marsala* City (ED50-UTM33N Coordinate Reference System); b) Direction of exposure and geographical fetch of *Lido Signorino* beach. c) Wave rose at the *Mazara del Vallo* buoy, related to the period 1 July 1989 to 5 June 2012

Figure 2. Anthropic pressure in the studied beach: a) central-northern beach, where buildings are at about 4-5 m from the shoreline and are reached by waves during sea-storms; b) central-southern beach, where buildings are noticeably farther from the shoreline

4 Validation of run-up assessment by means of field measurements: a *Marsala* beach

In order to validate the whole mathematical process used for run-up assessment, field measurements were performed (Lo Re et al., 2012a). The wave run-up on sandy beaches can be measured in several ways depending on the general aim and on the amount of details required.

5   Records of the shoreline positions can be obtained by resistance run-up gauges or by video-cameras, the technique adopted in present paper is based on a high frequency monitoring video system (Holman and Sallenger, 1985). Such kind of technique allows the acquisition of several images by means of a digital video camera. The choice of the position of the camera was a fundamental task because the camera has to shoot the whole studied area but at a little distance, in order to obtain the maximum level of detail from the recorded images. In particular, positions of the swash were measured on a transect across the beach, normal to the shore (Fig. 3). For this transect a line was built using rod at 0.5 m intervals. The first stake was a piezometer and it was next to the beach berm. The second stake of the line was placed at a distance of 5 m from the piezometer. The line stakes

on the beach profile was georeferenced using control points from a previous topographic survey. The video camera was placed at a distance of 10 m from the line of stakes (orthogonally), and it was used to record 240 minutes continuously. The shot videos were digitized in order to extract the wave run-up of each wave. When a wave reached a stake the data was recorded. The horizontal run-up distance were calculated starting from SWL obtained from water level inside the piezometer. Finally the corresponding run-up value was estimated by considering the beach profile. Each run-up measurement (R) was recorded in time windows of thirty minutes (eight windows in total) according to Nielsen and Hanslow (1991). For all recorded data, the Rayleigh distribution was fitted by using the least squares method. The application of the Rayleigh distribution to our data allowed estimation of the 2% run-up ($R_{2\%}$).

The expression of the Rayleigh cumulative distribution function is reported as follows:

$$F(R) = 1 - exp\left\{-\frac{(R - R_{100})^2}{L^2_{zwm}}\right\} \tag{9}$$

in which R_{100} is the value transgressed by 100% of the waves, i.e. the lower limit of the distribution, and L_{zwm} is the vertical scale of the distribution, i.e. the shape parameter.

Moreover to perform such a validation wave parameters from the buoy of *Mazara del Vallo* were used. In particular: 1) significant wave heights, H_s [m]; 2) peak period T_p [s] and 3) mean wave direction D_m [°N]. The extraction time period goes from 11:30 to 15:30 of 29 march 2011. The waves shown in Tab. 1 correspond to the sea states recorded by the buoy half-hourly.
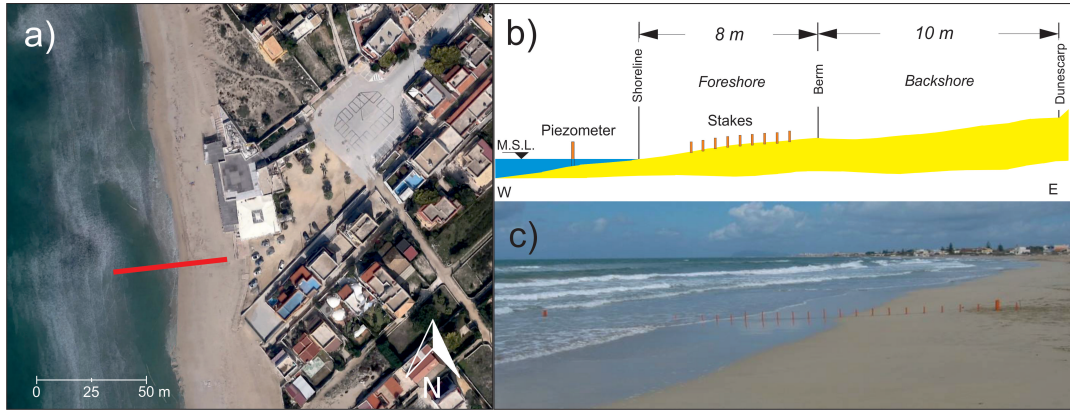
Figure 3. Plan view (a) cross section sketch (b) and beach profile (c) of the reference transect 45 (see following Section) for the run-up measurements at *Lido Signorino* beach

The obtained wave run-up are reported in Tab. 1. Such a table also shows, for each time window, the results obtained with the empirical formula by Nielsen and Hanslow (1991). The $R_{2\%}$ run-up determined by means of the Rayleigh distribution of field measurements is also shown.

Table 1. $R_{2\%}$ run-up comparison between field measurements, numerical model (Lo Re et al., 2012b) and empirical formula (Nielsen and Hanslow, 1991)

Wave#	Offshore H_s [m]	T_p [s]	Measured $R_{2\%}[m]$	Boussinesq $R_{2\%}[m]$	error [%]	Nielsen and Hanslow (1991) $R_{2\%}[m]$	error [%]
1	1.13	6.13	0.89	0.90	0.46	0.57	35.95
2	1.05	7.27	0.93	0.91	2.86	0.80	14.65
3	1.07	5.94	0.86	0.82	5.26	0.62	28.58
4	1.04	7.18	0.84	0.84	1.08	0.84	1.06
5	1.03	7.25	0.89	0.87	2.78	0.80	10.39
6	1.10	7.26	0.89	0.89	0.28	0.83	6.96
7	0.99	6.93	0.91	0.82	8.95	0.68	24.55
8	1.05	6.33	0.91	0.91	0.83	0.70	22.76
				mean	2.81		18.11

The analysis of the 2% run-up ($R_{2\%}$) highlights that both methods give acceptable results. In particular, the numerical model has an average percentage error of 2.81% and the empirical formula gives an average percentage error of 18.11%. The numerical Boussinesq model gives overall result closer to the field measurements and, for this reason, it was chosen for simulations of wave run-up in this study.

5   Method application and results

Five orthorectified aerial images were used to assess time variations of the shoreline position during the 1994–2007 time span (Table 2). Each image was georeferenced (WGS84 - UTM 33N) by 6-10 evenly spaced ground points. For each observation year, these images were used to form a photo-mosaic covering the whole coast studied. The shoreline relating to a photo-mosaic was traced and digitized manually using the wet/dry proxy, as suggested by Virdis et al. (2012) for dissipative beaches of the Mediterranean Sea.

Table 2. Characteristics of the aerial images used for the analysis of the case study

Images name	Data	Spatial resolution (m)	Film	Altitude fly [m]
Volo Italia 1994	07 June 1994	1	Black and white	11 500
Volo Italia IT2000	13 May 1999	1	Colour	6 000
Acquater	15 October 2000	4	Colour	3 000
Volo Italia IT 2006	29 September 2006	0.5	Colour	3 000
ECW 2007	16 September 2007	0.5	Colour	3 000

In order to reconstruct waves conditions at the day the aerial photos were made (Table 4), data recorded from the Mazara del Vallo buoy were analysed (Fig. 4). In particular, 3 hourly wave parameters were used for a total of 40 sea states for 5 days (each day has its specific beach profile, wave and tide). Every single sea state (see Table 4) was then propagated throughout the numerical domain by SWAN in stationary mode (Fig. 4). At the 5 m bathymetric line, the wave spectrum output of SWAN was used to generate a wave time-series (Table 4), which in turn was used as input to the Boussinesq model to assess the wave run-up in 26 sections. Table 3 shows the average slope for each day analysed. Therefore, 1 040 (26 sections × 40 sea state × 5 days) near-shore simulations were conducted for each offshore wave.

The considered sections (Fig. 4) are distinguished from the transects (discussed later) by an S preceding the number. In addition to the 26 sections, 68 transects orthogonal to the present shoreline (Fig. 4) were generated (with DSAS application) at about 50 m from one another to better analyse the shoreline changes and the related erosion/accretion rates between the transects themselves.

Table 3. Average beach slope in the analysed days

Section#	Slope	α [°]	Section#	Slope	α [°]
1	11.55	4.95	14	8.64	6.61
2	10.55	5.42	15	8.48	6.72
3	10.07	5.67	16	8.14	7.01
4	11.44	4.99	17	12.38	4.62
5	10.80	5.29	18	11.12	5.14
6	11.53	4.96	19	21.93	2.61
7	13.62	4.20	20	15.48	3.70
8	11.79	4.85	21	10.98	5.21
9	14.64	3.91	22	23.47	2.44
10	10.79	5.30	23	18.15	3.15
11	15.80	3.62	24	17.99	3.18
12	7.93	7.19	25	15.67	3.65
13	9.22	6.19	26	15.70	3.64

Table 4: Data and results of the simulations relating to the five aerial surveys: day considered for wave data processing, offshore wave data used as input for SWAN, and SWAN output used as Boussinesq-model input

Survey Date	Offshore wave data → SWAN-input			SWAN out → Boussinesq in	
[YYYY MM DD HH]	H_s [m]	$T_p(H_s)$ [s]	Dir [°]	H_s [m]	T_p [s]
1994 06 07 00	1.00	6.30	279	0.82	6.20
1994 06 07 03	0.90	5.90	276	0.75	6.00
1994 06 07 06	0.90	6.70	278	0.72	6.48
1994 06 07 09	0.80	6.30	280	0.68	6.23
1994 06 07 12	0.90	6.30	282	0.72	6.20
1994 06 07 15	0.90	4.50	289	0.80	4.49
1994 06 07 18	0.70	4.20	287	0.61	4.13
1994 06 07 21	0.60	5.60	281	0.50	5.51
1999 05 13 00	0.20	2.30	306	0.20	2.29
1999 05 13 03	0.20	4.80	268	0.17	4.71
1999 05 13 06	0.20	5.00	270	0.17	4.86
1999 05 13 09	0.20	4.00	324	0.19	3.95
1999 05 13 12	0.26	4.09	318	0.24	4.07
1999 05 13 15	0.32	4.18	313	0.29	4.13
1999 05 13 18	0.38	4.27	307	0.34	4.18
1999 05 13 21	0.44	4.35	302	0.39	4.25
2000 10 15 00	2.74	7.10	110	2.22	7.11
2000 10 15 03	2.02	6.70	154	1.91	6.67
2000 10 15 06	1.50	6.70	146	1.63	6.67
2000 10 15 09	1.30	6.70	177	1.28	6.67
2000 10 15 12	1.27	6.70	183	1.21	6.67
2000 10 15 15	1.24	6.70	189	1.14	6.67
2000 10 15 18	1.21	6.70	196	1.08	6.67
2000 10 15 21	1.18	6.70	202	1.05	6.67
2006 09 29 00	0.65	6.70	277	0.53	6.65
2006 09 29 03	0.62	5.70	258	0.49	5.68
2006 09 29 06	0.62	5.60	268	0.54	5.56
2006 09 29 09	0.57	4.76	276	0.52	4.77
2006 09 29 12	0.52	5.13	295	0.44	5.05

Continued on next page

Table 4: Data and results of the simulations relating to the five aerial surveys: day considered for wave data processing, offshore wave data used as input for SWAN, and SWAN output used as Boussinesq-model input

Survey Date	Offshore wave data → SWAN-input			SWAN out → Boussinesq in	
[YYYY MM DD HH]	H_s [m]	$T_p(H_s)$ [s]	Dir [°]	H_s [m]	T_p [s]
2006 09 29 15	0.45	4.50	278	0.37	4.49
2006 09 29 18	0.37	4.50	264	0.32	4.47
2006 09 29 21	0.32	4.55	261	0.29	4.50
2007 09 16 00	0.43	5.90	202	0.38	5.90
2007 09 16 03	0.37	6.70	215	0.33	6.63
2007 09 16 06	0.36	4.76	226	0.32	6.62
2007 09 16 09	0.35	5.41	232	0.31	6.49
2007 09 16 12	0.30	4.44	222	0.27	4.42
2007 09 16 15	0.34	4.76	187	0.31	4.63
2007 09 16 18	0.32	2.17	181	0.31	4.64
2007 09 16 21	0.40	3.51	190	0.39	3.45

Concluded

The Boussinesq wave propagation on 26 sections produced a number of run-up values that were then processed, obtaining the 2% wave run-up ($R2_{\%,i}$) and the run-up standard deviation $\sigma_{wr,i}$ (i = 1, 2, ..., 26) relating to each survey day (Fig. 5). Comparison between the run-up values and the standard deviation indicates, for each year, consistency between the $R_{2\%}$ and $\sigma_{wr,i}$ trends (Fig. 5). The wave run-up errors σ_{wr} (Eq. (8)) were summarized Table 5, together with the other uncertainties.

5   For each day with measurements, the standard deviation of the tide measurements (S_{td}) was first computed and then the standard deviations of the horizontal tidal fluctuations of the 26 sections were evaluated by Eq. (8). As is well known, tide fluctuation measurements include the meteorological effects.

Table 5. Standard deviations S_{td} of the tide fluctuations gauged at near station and the related tide uncertainties σ_{td} for *Lido Signorino* beach

Date	07 June 1994	13 May 1999	15 October 2000	29 September 2006	16 September 2007
S_{td} [m]	0.09	0.10	0.10	0.09	0.09
σ_{td} [m]	1.31	1.37	1.39	1.28	1.20

Based on the uncertainties (Table 6), the five shoreline rate-of-change indices mentioned earlier were evaluated using DSAS for each of the 68 transects. Indices WLR, EPR and LRR (Fig. 6) and indices NSM and SCE (Fig. 7) were plotted, with positive index values indicating shoreline accretion and negative values indicating recession.
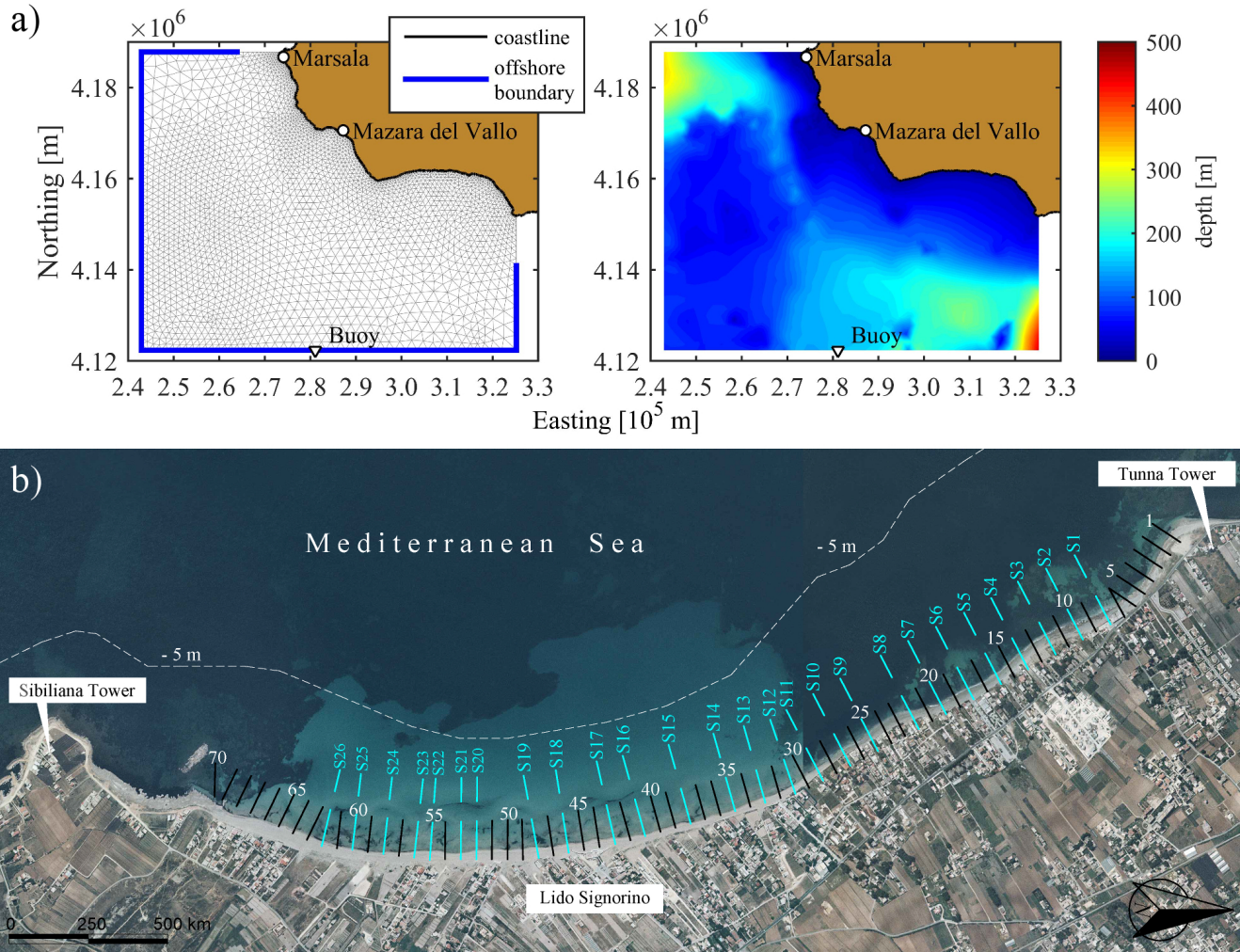
Figure 4. a) The unstructured mesh of the numerical domain (Monteforte et al., 2015). The blue bold line in the left panel represents the domain boundary along which the offshore wave conditions were imposed; The left panel represents the bathymetry of studied area); b) Location of the 26 sections chosen for the run-up analysis; each section is identified by a number preceded by S that distinguishes them from the transects, identified by a number only
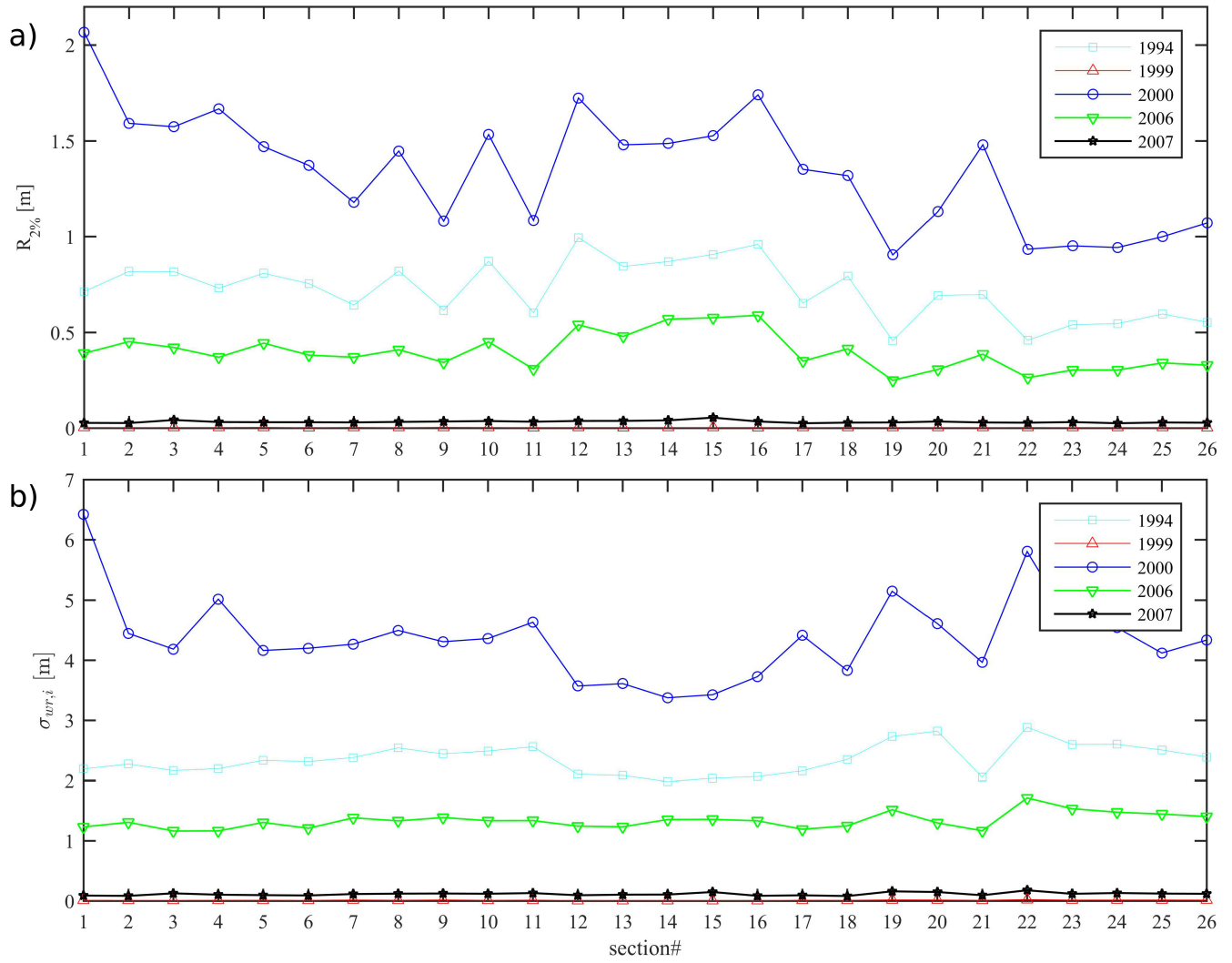
Figure 5. a) $R_{2\%}$ of the wave run-up output of Boussinesq model; b) standard deviation of the shoreline movement due to wave swash

Table 6. Uncertainties determined for the shoreline position [m]

Date	07 June 1994	13 May 1999	15 October 2000	29 September 2006	16 September 2007
σ_d	4.10	4.10	11.00	0.60	2.00
σ_p	1.00	1.00	4.00	0.50	0.50
σ_r	1.00	1.00	4.00	0.50	0.50
σ_{co}	1.00	1.00	4.00	0.00	0.00
σ_{wr}	2.41	0.01	4.50	1.36	0.12
σ_{td}	1.31	1.37	1.39	1.28	1.12
$\sigma_T(eq.(6))$	**5.23**	**4.66**	**13.83**	**2.09**	**2.40**

6 Discussions

6.1 comparison of shoreline rates of change

The trend differences in the five indices showed that variations among WLR, EPR, and LRR (Fig. 6a) are consistent, exhibiting generally similar trends both on accretion and on recession. Several accretion zones are clearly distinguishable in transects 12-13, 33-40, 47, and 65-67. The accretion rate is about 0.6 m year^{-1} for transect 47, 0.51 m year^{-1} for transects 12-13, and 1.0 m year^{-1} in transects 33-40, 47, and 65-67. By contrast, a recession is evident for transects 56-64, with a rate about –2.5 m year^{-1}, as well as for transects 48-50 of –1.6 m year^{-1}. For transects 20-22 and 40-43, lower recession rates of –1.18 and –1.28 m year^{-1}, respectively, are observed. In contrast to the other indices, NSM and SCE often present opposing trends (Fig. 6b), in which a relative maximum of one may correspond to a relative minimum of the other. This pattern depends on the different definitions of the two indices, but disparate conclusions can be drawn if one or the other criterion is adopted. Indeed SCE represents the total change in shoreline movement for all available shoreline positions and is not related to their dates. Fig 6b shows that NSM trend on the whole is consistent with the other indices trend (Fig 6a), except for transects 36-37 and 44-45. The lowest shoreline indices values (stable areas) were generally localized in transects from 3 to 9 (8 local maximum), from 22 to 34 (24 local maximum) and from 50 to 55.

In particular, in transects 12-13 a local deposition cusp was detected. The studied beach is not characterized by a rhythmic morphology, but massive presence of beach cusps could produce erroneous results as mentioned by Anfuso et al. (2016).

Transects 51 and 55 proved to be affected by even lower shoreline movements, despite considerable anthropogenic disturbances of the dunes, this for all the indexes showed in Fig 6a,b. Unlike the SCE index, the NSM trend (Fig. 6b) showed a reliable average equilibrium between beach accretion and recession, although in transects 56-64 a noticeable general recession occurs, in accordance with EPR, WLR, and LRR results (Fig. 6a).

Finally, the NSM indices relating to each period between two consecutive surveys were compared to highlight the shoreline evolution at each transect along the whole period 1994–2007 (Fig. 7), showing that accretion periods alternated with recession periods at each transect. In a few transects (e.g., transects 11 and 19) NSM was effectively unchanged, whereas in many

others it changed noticeably from one period to another. Moreover, during 2006–2007, accretion prevailed over recession along the entire beach, whereas recession was prevalent during 2000–2006, and during 1994–1999 and 1999–2000, accretion and recession basically balanced each other. The different behaviours (higher or lower accretion or recession) of different beach stretches observed in a given period followed the specific beach conformation of the stretches as well as the presence of

5 *Posidonia oceanica* leaves deposits. Note that all the indices considered detected higher shoreline changes in transects 58-68, where vast deposits of *Posidonia oceanica* leaves were present.
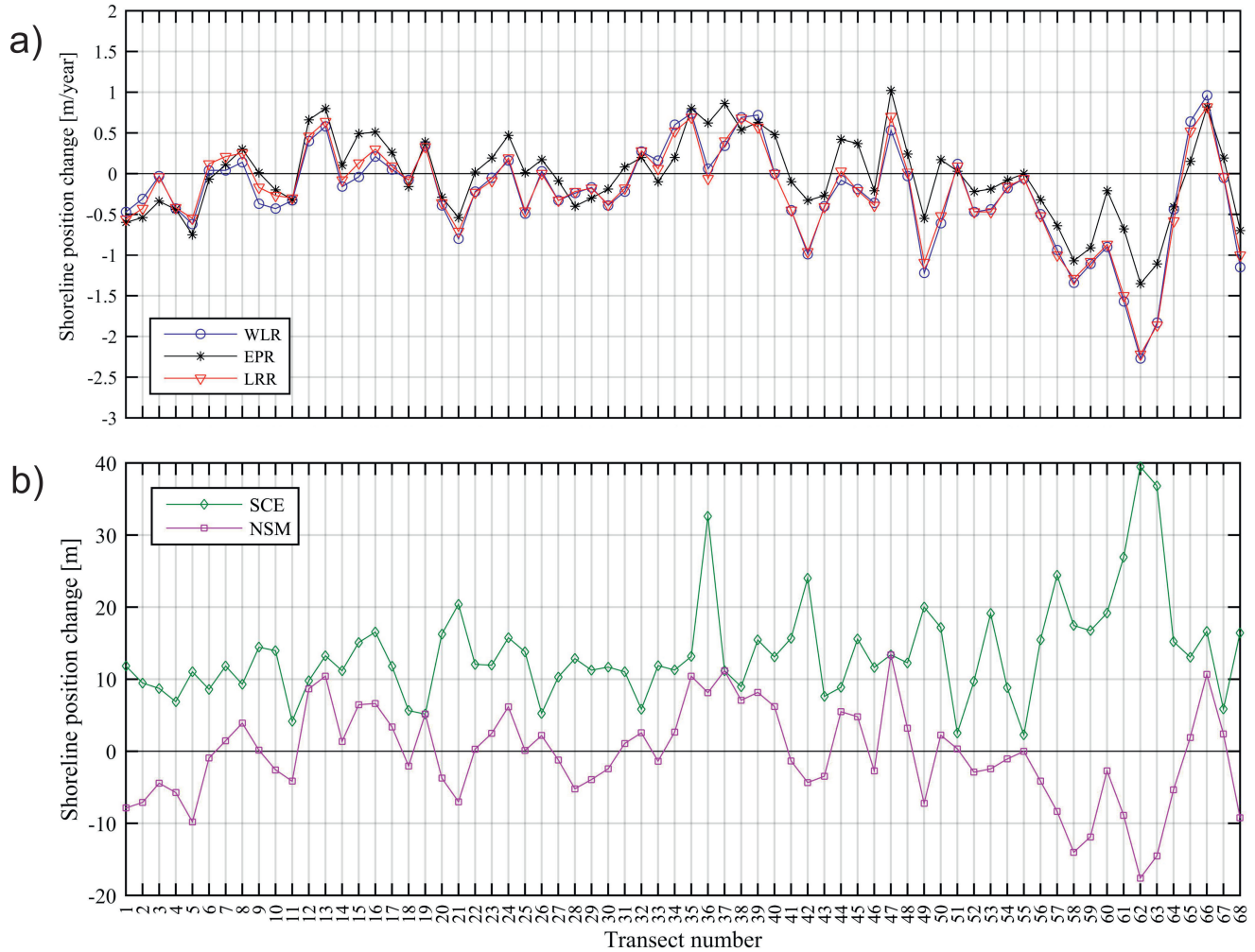
Figure 6. a) comparison among the change-rate of the shoreline position at each transect during the studied period, expressed by: End Point Rate (EPR), Linear Regression Rate (LRR), and Weighted Linear Regression rate (WLR); b) Comparison between the Net Shoreline Movement (NSM) and Shoreline Envelope of Changes (SCE) during the studied period
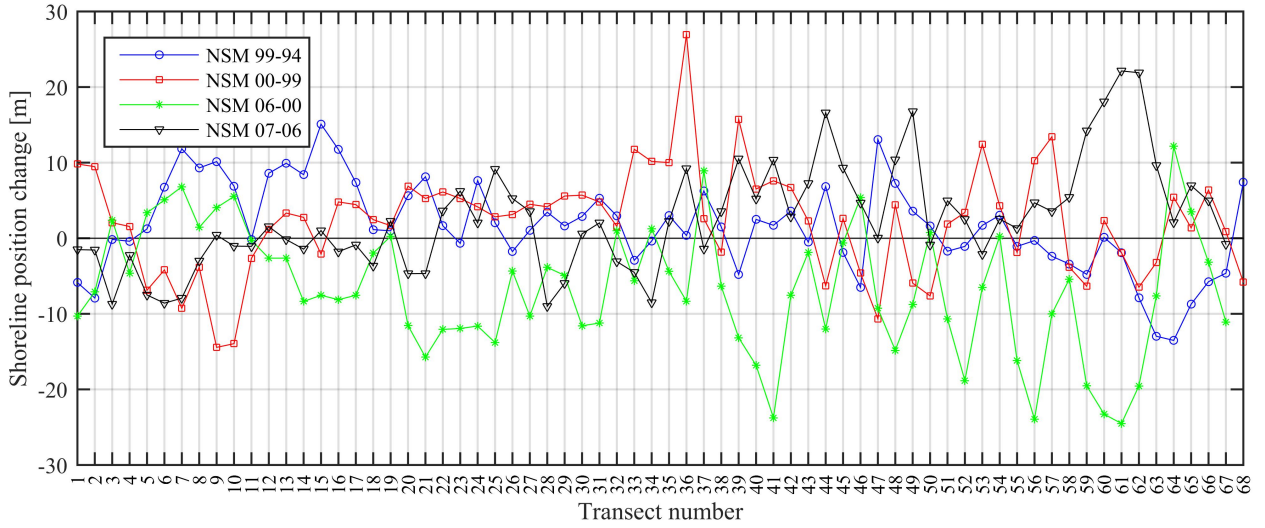
Figure 7. Comparison between the Net Shoreline Movement (NSM) relating to each period between two consecutive surveys

7   Conclusions

To analyse beaches by aerial images utilizing DSAS or similar applications, technicians usually neglect positioning uncertainties or assess them by means of empirical formulas without the use of hydraulic models. In this study, a new approach was adopted that assesses positioning uncertainties by analysing wave motion and tide effects.

5   The hydraulic models used in our methodological approach consist of a nearshore model (SWAN) and a more accurate dispersive model (Boussinesq) that provides a more accurate description of the hydrodynamic in the nearshore area, a fundamental step to estimate the oscillation of the shoreline. The proposed method can be used in all types of coastal areas (steep beaches, gentle slope beach etc.) and can reproduce the hydrodynamic of a large area, not just the hydrodynamic of one point. Moreover, the models can reproduce most all wave propagation effects (diffraction, refraction, reflection, shoaling, breaking,

10   etc.). The diachronic analysis on *Lido Signorino* shows a low shoreline variability, except for the most southern coastal stretch that has a high variability due to anthropic and natural causes.

The methodology adopted here provides high accuracy in wave run-up calculation, resulting in a more accurate σ_{wr} error estimation as highlighted from comparison of present model with in situ run-up measurements(see Section 4).

Using an application like DSAS that neglects or underestimates the σ_{wr} error may prevent determining if a beach is in

15   erosion or accretion, and a retreat rate close to the total uncertainty would not be acceptable. Furthermore, method accuracy is valuable in beach monitoring and management, especially when more sustainable methods are needed to sustain coastal resources. An integrated management of the coasts must be interdisciplinary and consider the dynamic process of the beaches, mainly when the beaches are largely urbanized and anthropized.

Acknowledgements. We thank Gino Dardanelli for assistance with topographic survey of the studied area, and for sharing with us his expertise in topographic measurements. We would like to express our gratitude to Giovanni Battista Ferreri for sharing his pearls of wisdom with us during the course of this research. We thank Massimiliano Monteforte for his comments.

References

Anfuso, G., Pranzini, E., and Vitale, G.: An integrated approach to coastal erosion problems in northern Tuscany (Italy): littoral morphological evolution and cell distribution, Geomorphology, 129, 204–214, 2011.

Anfuso, G., Bowman, D., Danese, C., and Pranzini, E.: Transect based analysis versus area based analysis to quantify shoreline displacement: spatial resolution issues, Environmental monitoring and assessment, 188, 1–14, 2016.

Boak, E. H. and Turner, I. L.: Shoreline definition and detection: a review, Journal of coastal research, 21, 688–703, 2005.

Booij, N., Ris, R., and Holthuijsen, L. H.: A third-generation wave model for coastal regions: 1. Model description and validation, Journal of geophysical research: Oceans, 104, 7649–7666, 1999.

Bush, D. M., Neal, W. J., Young, R. S., and Pilkey, O. H.: Utilization of geoindicators for rapid assessment of coastal-hazard risk and mitigation, Ocean & Coastal Management, 42, 647–670, 1999.

Cooper, J., Anfuso, G., and Del Río, L.: Bad beach management: European perspectives, Geological Society of America Special Papers, 460, 167–179, 2009.

Dolan, R., Hayden, B. P., May, P., and May, S.: The reliability of shoreline change measurements from aerial photographs, Shore and Beach, 48, 22–29, 1980.

Dolan, R., Fenster, M. S., and Holme, S. J.: Temporal analysis of shoreline recession and accretion, Journal of coastal research, 7, 723–744, 1991.

Douglas, B. C. and Crowell, M.: Long-term shoreline position prediction and error propagation, Journal of Coastal Research, 16, 145–152, 2000.

Fletcher, C., Rooney, J., Barbee, M., Lim, S.-C., and Richmond, B.: Mapping shoreline change using digital orthophotogrammetry on Maui, Hawaii, Journal of Coastal Research, SI 38, 106–124, 2003.

Genz, A. S., Fletcher, C. H., Dunn, R. A., Frazer, L. N., and Rooney, J. J.: The predictive accuracy of shoreline change rate methods and alongshore beach variation on Maui, Hawaii, Journal of Coastal Research, 23, 87–105, 2007.

Griggs, G. B.: The impacts of coastal armoring, Shore and beach, 73, 13–22, 2005.

Holman, R. A. and Sallenger, A.: Setup and swash on a natural beach, Journal of Geophysical Research: Oceans, 90, 945–953, 1985.

Holthuijsen, L., Booij, N., and Ris, R.: A spectral wave model for the coastal zone, in: Ocean Wave Measurement and Analysis, edited by Magoon, O. T. and Hemsley, J. M., pp. 630–641, ASCE, 1993.

Hunt, I. A.: Design of sea-walls and breakwaters, Transactions of the American Society of Civil Engineers, 126, 542–570, 1959.

Lo Re, C., Manno, G., Viviano, A., and Foti, E.: Field run-up measurements: calibration of a physically based lagrangian shoreline model, in: Coastal Engineering Proceedings, vol. 1, pp. 1–14, 2012a.

Lo Re, C., Musumeci, R. E., and Foti, E.: A shoreline boundary condition for a highly nonlinear Boussinesq model for breaking waves, Coastal Engineering, 60, 41–52, 2012b.

Manca, E., Pascucci, V., Deluca, M., Cossu, A., and Andreucci, S.: Shoreline evolution related to coastal development of a managed beach in Alghero, Sardinia, Italy, Ocean & coastal management, 85, 65–76, 2013.

Manno, G., Lo Re, C., and Ciraolo, G.: Shoreline detection in gentle slope Mediterranean beach, in: Proceedings of the 5th SCACR: International Short Conference on Applied Coastal Research, 2011.

Manno, G., Anfuso, G., Messina, E., Williams, A. T., Suffo, M., and Liguori, V.: Decadal evolution of coastline armouring along the Mediterranean Andalusia littoral (South of Spain), Ocean & Coastal Management, 124, 84–99, 2016.

Monteforte, M., Lo Re, C., and Ferreri, G.: Wave energy assessment in Sicily (Italy), Renewable Energy, 78, 276–287, 2015.

Moore, L. J.: Shoreline mapping techniques, Journal of Coastal Research, 16, 111–124, 2000.

Moore, L. J., Ruggiero, P., and List, J. H.: Comparing mean high water and high water line shorelines: should proxy-datum offsets be incorporated into shoreline change analysis?, Journal of Coastal Research, 22, 894–905, 2006.

5 Nielsen, P. and Hanslow, D. J.: Wave runup distributions on natural beaches, Journal of Coastal Research, 7, 1139–1152, 1991.

Pajak, M. J. and Leatherman, S.: The high water line as shoreline indicator, Journal of Coastal Research, 18, 329–337, 2002.

Phillips, M. R. and Jones, A. L.: Erosion and tourism infrastructure in the coastal zone: Problems, consequences and management, Tourism Management, 27, 517–524, 2006.

Rangel Buitrago, N. G. and Anfuso, G.: Risk Assessment of Storms in Coastal Zones: Case Studies from Cartagena (Colombia) and Cadiz
10   (Spain), Springer International Publishing, 2015.

Ris, R., Holthuijsen, L., and Booij, N.: A third-generation wave model for coastal regions: 2. Verification, Journal of Geophysical Research: Oceans, 104, 7667–7681, 1999.

Robertson, W., Whitman, D., Zhang, K., and Leatherman, S. P.: Mapping shoreline position using airborne laser altimetry, Journal of Coastal Research, 20, 884–892, 2004.

15 Romine, B. M. and Fletcher, C. H.: A summary of historical shoreline changes on beaches of Kauai, Oahu, and Maui, Hawaii, Journal of Coastal Research, 29, 605–614, 2012.

Rooney, J., Fletcher, C., Barbee, M., Eversole, D., Lim, S.-C., Richmond, B., and Gibbs, A.: Dynamics of sandy shorelines in Maui, Hawaii: consequences and causes, Coastal Sediments 2003 Proceedings,(Clearwater Beach, Florida), 2003.

Rusu, E.: Wave energy assessments in the Black Sea, Journal of marine science and technology, 14, 359–372, 2009.

20 Stancheva, M., Rangel-Buitrago, N., Anfuso, G., Palazov, A., Stanchev, H., and Correa, I.: Expanding level of coastal armouring: case studies from different countries, Journal of Coastal Research, SI 64, 1815, 2011.

Stockdon, H. F., Sallenger Jr, A. H., List, J. H., and Holman, R. A.: Estimation of shoreline position and change using airborne topographic lidar data, Journal of Coastal Research, 18, 502–513, 2002.

Thieler, E. R., Himmelstoss, E. A., Zichichi, J. L., and Ergul, A.: The Digital Shoreline Analysis System (DSAS) version 4.0-an ArcGIS
25   extension for calculating shoreline change, Tech. rep., US Geological Survey, 2009.

U.S. Army: Coastal Engineering Manual.Engineer Manual 1110-2-1100, US Army Corps of Engineers, Washington, DC, 2008.

Virdis, S. G., Oggiano, G., and Disperati, L.: A geomatics approach to multitemporal shoreline analysis in Western Mediterranean: the case of Platamona-Maritza beach (northwest Sardinia, Italy), Journal of Coastal Research, 28, 624–640, 2012.